Paper No.
16413

Effect of Time on High Temperature Naphthenic Acid and Sulfur Corrosion of Carbon Steel under Continuous Oil Flow Conditions

Prince Kumar Baranwal
Department of Chemical Engineering, National Institute of Technology Andhra Pradesh
Tadepalligudem, Andhra Pradesh, 534101, India

Winston Robbins, Gheorghe Bota
Institute for Corrosion and Multiphase Technology, Ohio University
342 West State Street
Athens, Ohio, 45701
USA
E-mail: bota@ohio.edu

ABSTRACT

The present research study investigated the effect of time duration on crude fractions corrosivity in high temperature experiments performed in a flow through apparatus with continuous replenishment. The experiments duration varied from 1 to 7 days and assessed the corrosivity as function of time for three different vacuum gas oils (VGO). Along with the metal loss evaluations, naphthenic (NAP) acids and sulfur species concentrations were monitored by potentiometric titrations and X-Ray Fluorescence spectrometry (XRF), respectively. Corrosion damage of the metal surfaces and the scales formed on them were analyzed by Scanning Electron Microscopy (SEM) and Energy Dispersive X-Ray Spectroscopy (EDS). The study provided valuable information on NAP acids and sulfur species corrosivity and their chemical evolution during long time experiments by integrating metal losses with feed and product analyses.

Key words: naphthenic acid corrosion, sulfur corrosion, crude fractions, time effect, high temperature

INTRODUCTION

Naphthenic (NAP) acid and sulfur corrosion is one of the major problems in refinery, especially with the increase in processing of opportunity crudes.[1-5] These low quality, discounted, heavy crude oils contain high concentrations of NAP acids and sulfur based corrosive species. It is reported that the presence of these species leads to detrimental effect on equipment integrity and process unit reliability.[2-6] Thus, in refineries, special procedures and strategies (for instance, crude blending) have to be adopted when processing these crudes, in order to mitigate the corrosive effects associated with NAP acid and sulfur

components.[7] Consequently, to be able to make such decisions for mitigation, understanding the corrosion reaction mechanism of NAP acid and sulfur corrosion is imperative.

NAP acids concentration in oil is measured by titration and it is commonly named as Total Acid Number (TAN) expressed as mg of KOH necessary to neutralize 1g of oil. NAP acids are highly corrosive when oil is distilled and reach their highest effect at a temperature range of 220 - 400°C when they attack the metal and form oil soluble iron naphthenates. In the same temperature range of NAP acids, the sulfur compounds in oil are also corrosive with their highest activity peak around 425°C. Sulfur compounds in oil thermally decompose at these high temperatures and form hydrogen sulfide that reacts with metal generating iron sulfide (FeS), a solid crystalline corrosion product that builds up on metal surfaces as multilayered scales. Both of these corrosive species interact synergistically at high temperature and their combined effects are commonly considered to be described by the three reactions mentioned below:[1-3, 8]

$$Fe + 2RCOOH \rightarrow Fe(RCOO)_2 + H_2 \quad (1)$$

$$Fe + H_2S \rightarrow FeS + H_2 \quad (2)$$

$$Fe(RCOO)_2 + H_2S \leftrightharpoons FeS + 2RCOOH \quad (3)$$

NAP acids attack the metal as in reaction (1) and form oil soluble iron salts, while hydrogen sulfide interacts with the metal too (sulfidation) and generates the solid FeS - reaction (2). The two reactions (1) and (2) occur almost simultaneously and they are followed by reaction (3) when excess H_2S reacts with the iron naphthenates forming more FeS and regenerating the original NAP acids from their salts. Thus, the hydrogen sulfide by regenerating the NAP acids as in reaction (3) reintroduces them into the corrosive cycle of acids and S-compounds.

The corrosion mechanism due to NAP acid and sulfur compounds (NAP acid and sulfidic corrosion) has been intensively studied in the past.[2-11] Nevertheless, the mechanism associated with these species is still not clearly understood, although the effect of factors such as S/TAN ratio, temperature, molecular weight and structure of the corrosive species present in crude oil, were considered in the effort to understand the interaction between NAP acid and S-compounds. [6, 9-13] Jin et al. reported that the scale formed in corrosion experiments with real crude fractions consists mainly of iron sulfide (FeS) but it also includes a thin layer of iron oxide.[14] They also developed a mechanistic corrosion model of NAP acid and sulfur corrosion that includes the formation of the iron oxide layer for a fixed duration.

Most of the experimental data published in the literature and related to NAP acid corrosion were generated under static conditions in autoclaves or in glass equipment. This research work had as a main objective to study the NAP acids and sulfur corrosion at high temperature under continuous flow conditions, at different time intervals, and using real crude fractions. Three different vacuum gas oils (VGO) labeled as A1, B1 and C1 were evaluated using a special “flow through” apparatus at 343°C in experiments with durations of 24h to 168h (1 - 7 days). The TAN and total sulfur content of the three selected VGO are presented in Table 1. The metal samples and the scales formed on their surfaces in these experiments were analyzed by scanning electron microscopy (SEM) and energy dispersive X-ray spectroscopy (EDS).

Table 1: TAN and total S content (wt.%) of fractions selected for this study

VGO Fraction	TAN (mg KOH/g)	S (wt.%)
A1	8.30	0.75
B1	2.77	1.35
C1	1.51	1.92

EXPERIMENTAL PROCEDURE

Experimental Method

All experiments evaluating the corrosive effects of VGO for different time durations were performed in the Flow Through Mini-Autoclave (FTMA) which is a “flow through” apparatus that allows a constant refreshing of the corrosive species on specimens surface during the test. The very low oil flow rate in the FTMA and the specific design of this apparatus creates almost stagnant flow conditions at the specimen surface level. Thus, the FTMA testing conditions are similar to those of the static autoclave; however, the continuous oil flow in the FTMA reactor exposes the specimens to a constant concentration of corrosive species and prevents the accumulation of corrosion products. The effect of time duration on crude fractions corrosivity was assessed in the FTMA tests by measuring the samples corrosion rates, while periodically monitoring the evolution of TAN in every test. In addition, the total sulfur content and iron concentrations were determined periodically for one of the selected VGO. The structure, morphology, and the chemical composition of scales formed in every test on the samples were analyzed using the SEM/EDS.

Experimental Equipment

Figure 1 depicts a schematic representation of the FTMA “flow through” system used to test the carbon steel (CS) specimens under the experimental conditions mentioned in Table 2. The FTMA comprises of three feeding tanks, the reactor, two pumps - HPLC and gear pump, and a waste container where the used fluid is collected. The FTMA system also includes a three-way valve that is utilized for alternating the oil feeds if it is required by specific experimental procedures. In this study, only one vessel was used and filled with a VGO fraction that was pumped continuously from it to the FTMA reactor containing the CS specimens during testing. The temperature during experiments was controlled through a thermocouple inserted into the reactor up to the specimen location. A back-pressure valve was utilized to maintain pressure inside the reactor and to prevent the volatile species from vaporizing into the gaseous phase. Thus, the experiment is carried out only in liquid phase.

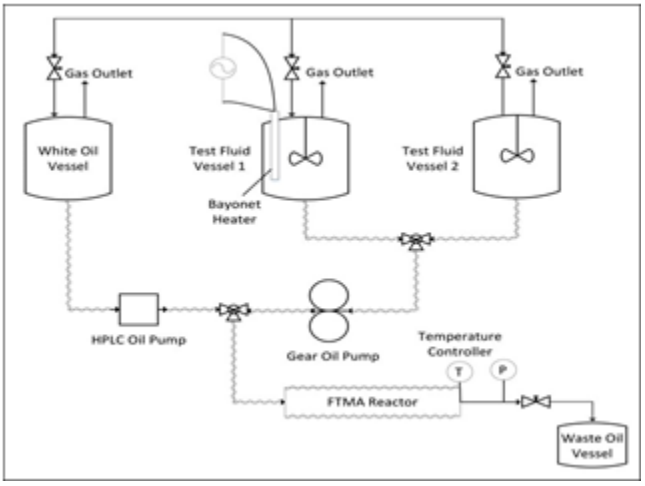

Figure 1: Schematic representation of the Flow Through Mini Autoclave (FTMA), a “flow through” apparatus.

In every experiment, initially, the polished steel specimens were placed inside the FTMA reactor which was then inserted into the apparatus flow system. The reactor with the specimens were heated gradually to 343°C with mineral oil (White Oil Vessel in Figure 1) being pumped through the reactor.

When the FTMA system reached the preset temperature of 343°C, the oil feed was switched from mineral oil to the experimental VGO fraction (Test Fluid Vessel 1 in Figure 1). The oil flow through the FTMA reactor was set to 1.5 cm^3/min for the VGO long experiments. At the end of the VGO experimental time phase, the flow was switched back to mineral oil and the FTMA system was flushed to remove completely the VGO from the reactor and the feeding lines. Then the FTMA was turned off and allowed to cool. Each experiment was performed using four steel specimens: two were dedicated for weight loss measurements, and two for SEM and EDS analysis.

The specimens and the corrosion by-product (scales) formed on them during the experiments were analyzed using the scanning electron microscopy JEOL JSM-6390 for the scale surface characterization and scale structure morphology in cross-sections. The EDS detector connected with SEM was employed to ascertain the chemical composition of the scales formed on the specimens.

Iron (Fe) and sulfur (S) concentrations in oil samples were measured using the X-Ray Fluorescence (XRF). The XRF analyzer PetraMax (XOS) is a high definition X-ray fluorescence (HDXRF) instrument that measures the S and Fe concentrations in oil samples according to ASTM D 4294.[15]

The acidity of the crude fractions was monitored during the experiments by measuring the TAN on samples collected on different time intervals. The TAN measurements were performed according to ASTM D664 using the Aquamax (GR Scientific) TAN titrator.[16]

Table 2: Experimental conditions in the FTMA experiments.

Test Fluid	**TAN** (mg KOH/g oil)	**Total Sulfur** (wt.%)	**T** (°C)	**Time** (h)	**Oil Flow Rate** (cm^3/min)	**P** (kPa)
Fraction A1	8.30	0.75	343	24, 48, 72, 168	1.5	791
Fraction B1	2.77	1.35	343	24, 48, 72, 168	1.5	791
Fraction C1	1.51	1.92	343	24, 48, 72, 168	1.5	791

Experimental Materials

The three VGO *i.e.* fractions A1, B1, and C1 were selected for this experimental work based on their performance in previous corrosion tests. The total sulfur (S) content (wt.%) and the TAN (mg KOH/g oil) of fractions A1, B1, and C1 are given in Table 2.

The specimens used in these FTMA experiments were made of UNS K03006 carbon steel (CS) and had a rectangular geometry with the specific dimensions; 16 mm X 15.2 mm X 0.6 mm with a central circular hole of 3.84 mm diameter. Table 3 presents the chemical composition of the CS UNS K03006 used to fabricate these specimens.

Prior to each experiment, the CS specimens were polished sequentially with 400 and 600 grit silicon carbide paper under isopropanol flush to prevent heating and oxidation of the specimens. After polishing, the specimens were rinsed with toluene and acetone, and dried under the flow of nitrogen gas. The geometrical dimensions of each specimen were measured with a caliper and recorded. The cleaned specimens were then weighed using an analytical balance and installed within the FTMA reactor. At the end of the experiment, the specimens were taken out of the reactor and processed for corresponding assessments - weight loss evaluation and SEM/EDS analysis. In weight loss evaluations, specimens were rinsed with toluene and acetone, and then the scale formed on their surfaces was removed mechanically by brushing them with a stiff plastic brush. The scale that survived on specimens after brushing was further removed chemically by immersing them into Clarke solution

(ASTM G 1-90) several times.[17] After every immersion in Clarke solution, the specimens were dried under nitrogen flush and weighed on the analytical balance.

Table 3: Chemical composition (wt.%) of carbon steel specimen.

C	Si	P	Mn	S	Cr	Cu	Ni	Mo	V	Fe
0.18	0.41	0.11	0.8	0.06	0.02	0.08	0.04	0.02	0.03	Balance

Corrosion Rates Evaluation

The corrosivity of VGO in FTMA experiments was evaluated by measuring the metal losses of specimens used in these tests. Based on specimen metal losses, the corrosion rates were calculated with equation (4) using the difference between specimen weight before and after the experiment. All corrosion rates are expressed in mm/y.

$$CR = \frac{(IW - FW)}{\rho_{Fe} \cdot A_c \cdot t} \cdot 24 \cdot 365 \cdot 1000 \quad (4)$$

where,

CR - corrosion rate [mm/y],
IW - initial weight (before the experiment) [kg],
FW - final weight (after final "clarking") [kg],
ρ_{Fe} - iron density [kg/m^3],
A_c - coupon area exposed to VGO fraction [m^2],
t - time of the experiment [h].

RESULTS AND DISCUSSION

Corrosion Rate Results

Corrosion rates of CS specimens used in these experiments provided a good information regarding the effect of testing duration on crudes corrosivity. Thus, the corrosion rates comparison in Figure 2 suggests that in general, for the three selected fractions their corrosivity decreased with time. However, in case of fractions A1 and B1 in short time testing, the 24h test interval did not influence their corrosivity and the corresponding corrosion rates were similar for the two considered time intervals *i.e.* 24h and 48h. Only when the test duration was increased to 72h and 168h respectively, there was a significant drop in corrosion rate values for the two fractions. In case of fraction C1 after a pronounced drop of corrosion rates on going from 24h to 48h test interval, their values remained the same in the 72h test and decreased further in the 168h test.

The corrosion rates measured in this set of experiments were also compared as a function of the crude fraction original TAN and total sulfur content. Comparison of corrosion rates with total sulfur as reference indicates that the higher was the total sulfur content in the crude fraction, the more corrosive it was regardless of the fraction TAN content or the experimental time duration. Hence, their corrosivity order was $CR_{A1} < CR_{B1} < CR_{C1}$.

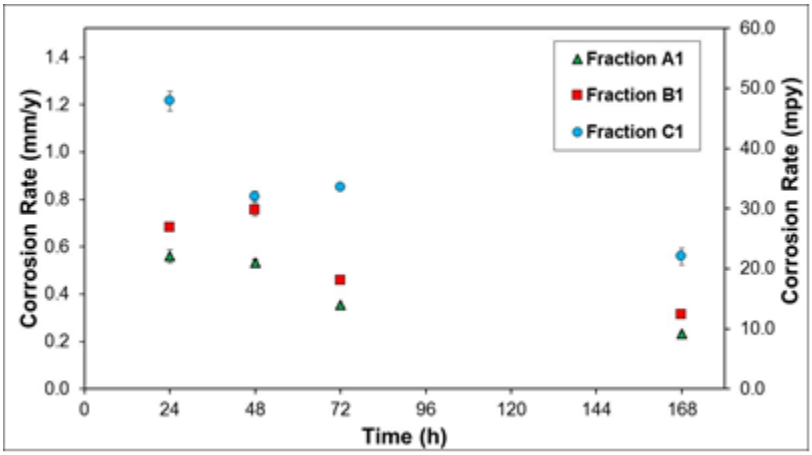

Figure 2: Corrosion rates plotted as function of time in FTMA experiments done at 343°C using fractions A1, B1, and C1.

Total Sulfur Content and Iron Concentration Monitoring Results – XRF Data

The XRF method is commonly used in oil industry to measure the concentrations of S and several metals present in crude oils. During this experimental work, an XRF analyzer was available for a short period of time and used to evaluate the total S content and iron concentrations in oil samples collected in two experiments done with fraction A1. For XRF analysis, oil samples were collected in two different experiments using fraction A1. The first set of samples were collected in the 24h experiment on following time intervals: 1, 2, 3, 4, 5, 6, 12, and 24 hours. The second set of samples were collected daily in the 168h (7 days) experiment, *i.e.* 1, 2, 3, 4, 5, 6, and 7 days. All oil samples were analyzed according to ASTM D 4294 with the XRF instrument.

The XRF data for S concentration presented in Figure 3 reveals that the oil S concentration decreases significantly in the first hour as compared to the initial value (0.75 wt.%), then increases also abruptly in the next hour (2h sampling), and continues to increase slowly but constantly for the next 4h (2 – 6h sampling) to values closer to the initial original value of total S content of fraction A1. This evolution of S content suggests that sulfur compounds reactions with the metal were very intense in the first hour and formed the FeS scale. As the FeS scale formed on the metal surface, it became a barrier for the diffusion of corrosive species in fraction A1 and reduced their reaction with the metal. The S concentrations measured in oil samples collected daily in the 168h (7 days) test are presented in Figure 4. The XRF data for S plotted in this figure suggest that S concentration does not change much during this 168h test as compared to initial total S concentration of fraction A1 (0.75 wt.%).

The evolution of Fe concentrations measured simultaneously with S concentrations (same oil samples), along the 24h test are shown in Figure 5. In the first hour of this test, the Fe concentration is very high, then in the following hour it starts to decrease reaching a low level after 3 hours, a level lower than the initial content of Fe in fraction A1. The XRF data plotted in Figure 5 indicates that the Fe concentration remains low and almost the same as the 3h value for the rest of the test duration. The Fe measured in oil samples is from iron naphthenates composition that are formed in the direct reaction of NAP acids with the metal. Therefore, the spike in Fe concentration revealed by the XRF data indicates an intense NAP acid attack on the metal during the first hour of the test. Further during the test, the decrease of Fe concentration indicates the NAP acid attack is reduced as their diffusion to the metal is blocked by the newly formed FeS scale. Thus, the XRF data for total S content and Fe concentration in oil offers a good information on scale formation and growth, and on NAP acid attack on metal surface.

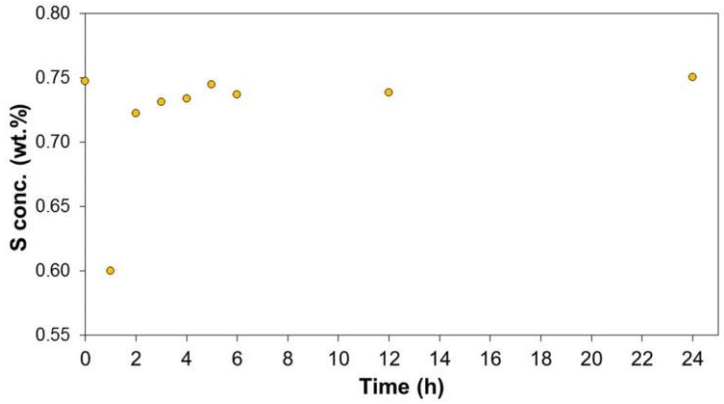

Figure 3: XRF data on S concentrations measured in oil samples collected on different time intervals in a 24 h experiment with fraction A1 (TAN = 8.30, S = 0.75 wt.%).

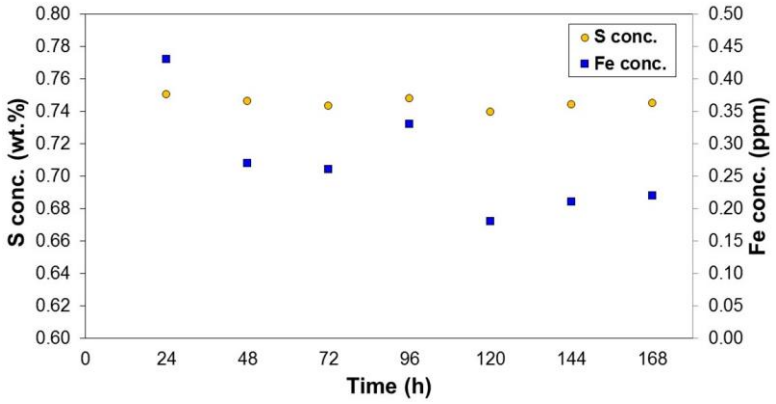

Figure 4: XRF data on S and Fe concentrations measured for fraction A1 oil samples collected on daily intervals in a 168 h (7 days) experiment with fraction A1 (TAN = 8.30, S = 0.75 wt.%).

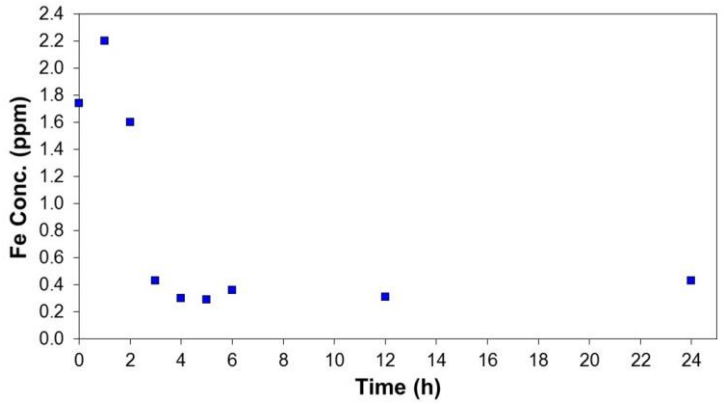

Figure 5: XRF data on Fe concentrations measured in oil samples collected on different time intervals in a 24 h experiment with fraction A1 (TAN = 8.30, S = 0.75 wt.%).

The S and Fe concentrations of samples collected in the 168h test with fraction A1 and measured with the XRF analyzer are presented in Figure 4. In case of the total S content, the plotted data in this figure

suggests that the S compounds ceased to react with the metal after the FeS scale was formed during the first hours of the test. The Fe concentrations plotted in the same Figure 4 suggest there was some variation in NAP acid activity on the 4th day of the test. This Fe concentration variation on the 4th day might suggest that the NAP acids were able to react with the metal probably through some defect of the scale (crack). However, this is only a hypothesis as the range of the measured Fe concentrations is very narrow and the XRF analysis cannot make a distinction between dissolved Fe in oil and chemically bonded Fe in naphthenates. Further experimental work is required to verify this hypothesis of NAP acids diffusion through scale imperfections during long time tests.

TAN Evolution Results

The reactivity of NAP acids was also evaluated in all these experiments by measuring the TAN in oil samples collected on different time intervals for all the three crude fractions. All TAN measurements were performed according to ASTM D664. In case of fraction A1, as XRF data was available for the Fe concentrations, TAN values were graphically presented and compared with Fe on the same plot in Figure 6. The variation in TAN values confirms the NAP acids reactivity with the metal that was suggested by the high Fe concentrations measured with the XRF. As the NAP acids react with the metal, the TAN value decreases with simultaneous increase in the concentration of Fe. This surge in the value of Fe concentration indicates the formation of iron naphthenates. Both TAN and Fe concentrations evolution suggest that the NAP acid attack on the metal is very intense during the first hour and it decreases as the acid diffusion through the FeS scale becomes more difficult.

Oil samples were collected for fractions B1 and C1 on the same time intervals as in the case of fraction A1 and TAN was evaluated for each sample. Comparison of TAN values measured in oil samples collected in the 24h tests with fractions A1, B1, and C1 (Figure 7) suggests that NAP acids in all of the three fractions reacted with metal in the first hours of the experiments and then their activity was reduced. The TAN evolution in case of A1 is more evident in Figure 7 as this fraction had the highest TAN (8.30) of the three VGO. The TAN values measured in the first hours of experiments with fractions B1 and C1 indicate a low activity of NAP acids in these experiments. However, both B1 and C1 generated high corrosion rates in these experiments and had higher total S contents than A1. Therefore, it might be hypothesized that B1 and C1 high corrosivity was mainly caused by their S compounds and less by the NAP acids. Figure 8 compares the TAN values of all three fractions measured during the 168 h experiments. The TAN measurements performed after the first 12h of each experiment indicate that there was no significant NAP acids activity after the first 24h of these long-term experiments.

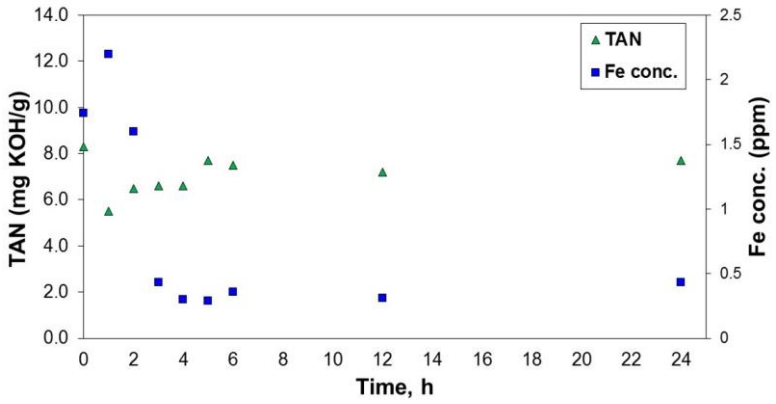

Figure 6: Comparison of TAN and Fe concentration measured in oil samples collected on different time intervals in a 24 h experiment with fraction A1 (TAN = 8.30, S = 0.75 wt.%).

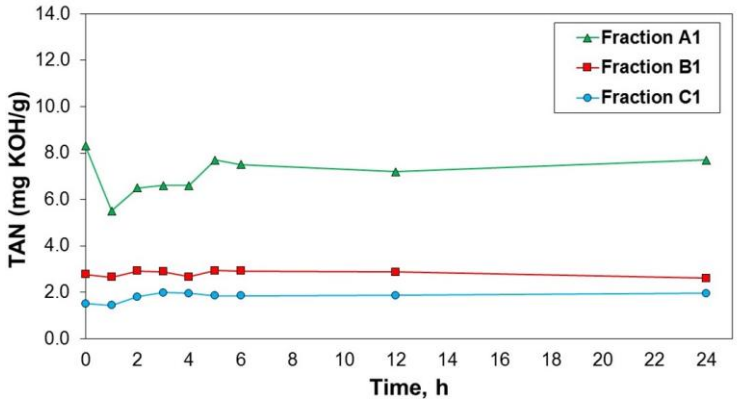

Figure 7: Comparison of TAN values of oil samples collected in 24 h experiments done with fractions A1, B1, and C1. (A1 - TAN = 8.30, S = 0.75 wt.%; B1 - TAN = 2.77, S = 1.35 wt.%.; C1 - TAN = 1.51, S = 1.92 wt.%).

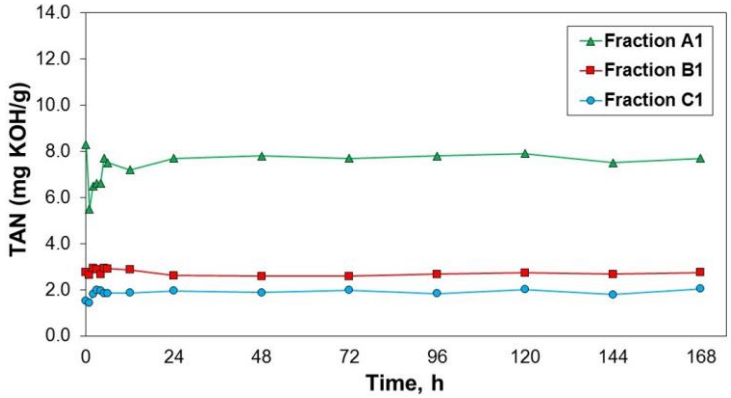

Figure 8: Comparison of TAN values of oil samples collected in 24h and 168h experiments done with fractions A1, B1, and C1. (A1 - TAN = 8.30, S = 0.75 wt.%; B1 - TAN = 2.77, S = 1.35 wt.%.; C1 - TAN = 1.51, S = 1.92 wt.%).

Scale Analysis

Scale Analysis in SEM Cross-Sections

The SEM and EDS analysis were used in addition to experimental corrosion rates and analytical XRF data to characterize the corrosive effects of fractions A1, B1, and C1. Figure 9 compares the SEM images of scales formed by fraction A1 on CS in experiments with different time durations (24 – 168h). The scales formed with A1 in 24h (a) and in 48h (b) tests consisted of successive layers with fragmented structures. The 72h and 168h test scales, Figure 9 (c) and (d), are also fragmented but no layering is visible. The scale thickness of the 168h scale is thicker than that of the 24h scale and the SEM image reveals a more irregular attack with deeper damages for the longer time test.

The SEM images for scales formed with fraction B1 are compared in Figure 10. All these scales formed with fraction B1 had a fragmented, multilayered structure. However, in this case with a moderate S/TAN

ratio, the changes in thickness follow a pattern opposite of that for the high S/TAN ratio of fraction A, *i.e.* the scale became thinner as the duration increased.

The SEM images of scales formed with fraction C1 are compared in Figure 11. Fraction C1 had the highest total S content of the three fractions and the scales it formed were very thick. Therefore, the SEM images of these scales presented in Figure 11 were collected at a lower magnification (2500X) than all previous images. Fraction C1 formed very thick multilayered scales in 24h and in 168h experiments. Similar structural characteristics were observed in the SEM images of the scales generated in 48h and in 72h tests, but they were not as thick as the other two test scales. It is difficult to characterize the corrosivity of the three fractions based only on the SEM images of the scales they formed. Therefore, additional EDS analysis was applied to these cross-sections.

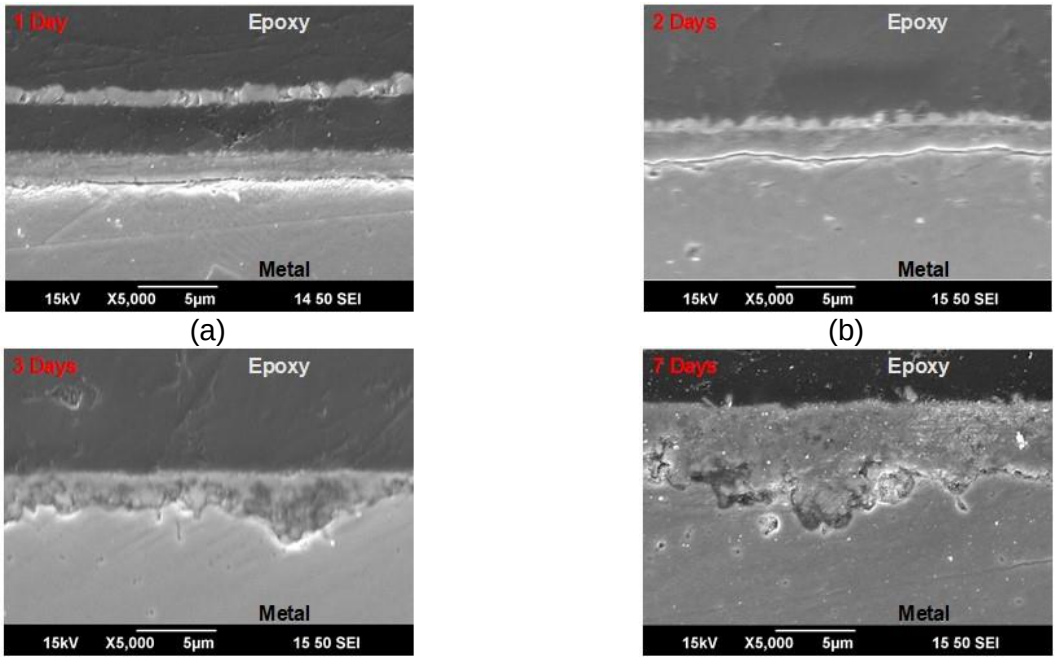

Figure 9: Cross-section SEM images of scales formed on CS with fraction A1 (TAN = 8.30, S = 0.75 wt.%) in 24h (a), 48h (b), 72h (c), and 168h (d) FTMA tests.

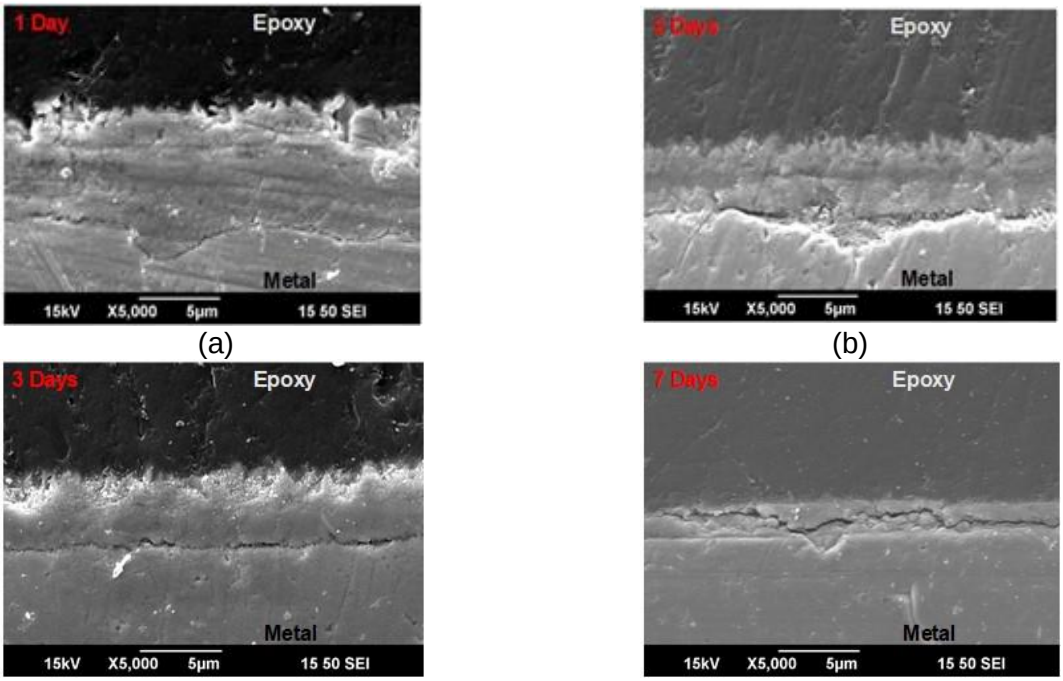

Figure 10: Cross-section SEM images of scales formed on CS with fraction B1 (TAN = 2.77; S = 1.35 wt.%) in 24h (a), 48h (b), 72h (c), and 168h (d) FTMA tests.

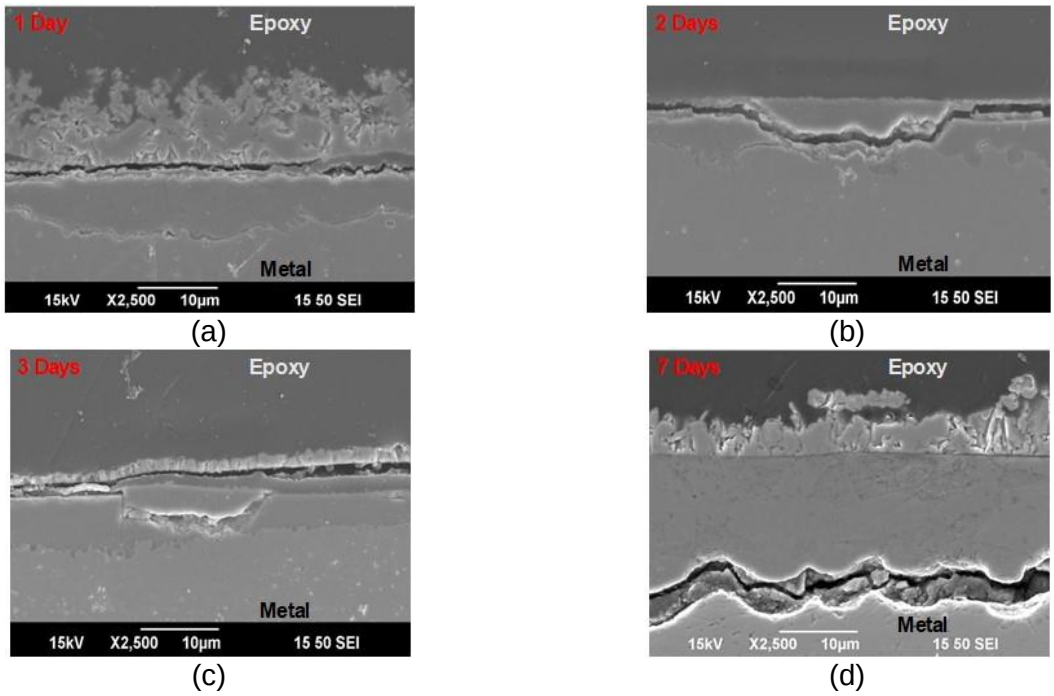

Figure 11: Cross-section SEM images of scales formed on CS with fraction C1 (TAN = 1.51; S = 1.92 wt.%) in 24h (a), 48h (b), 72h (c), and 168h (d) FTMA tests.

Scale Analysis - EDS Results

EDS line scanning analysis was performed on all cross-sections generated in the experimental work but only the most relevant comparisons were included in this paper. Thus, Figure 12 compares the SEM/EDS analyses of scales formed with fraction A1 in the 24h test (a) & (b) and in the 168h test (c) & (d), respectively. The SEM images in each case include the direction (in red) and the length (μm) of the EDS scanning. The SEM image of the 24h scale (a) shows a multilayered structure with the superficial layer delaminated from the rest of the scale. This scale consisted of FeS as the EDS scanning analysis across the specimen detected and identified S and Fe as main chemical elements. For the 168h (d) experiment similar EDS scanning analysis detected also S and Fe in the scale structure, but it also identified oxygen (O) in the same region where S was identified. This mixed composition of S, O, and Fe of the scale suggests that an iron oxide was formed in the scale. The formation of such iron oxide in scales generated by crude fractions at high temperature was described in several papers.[9-11] The formation of this oxide layer during the 168h test might explain the thicker scale found on the specimens at the end of this test.

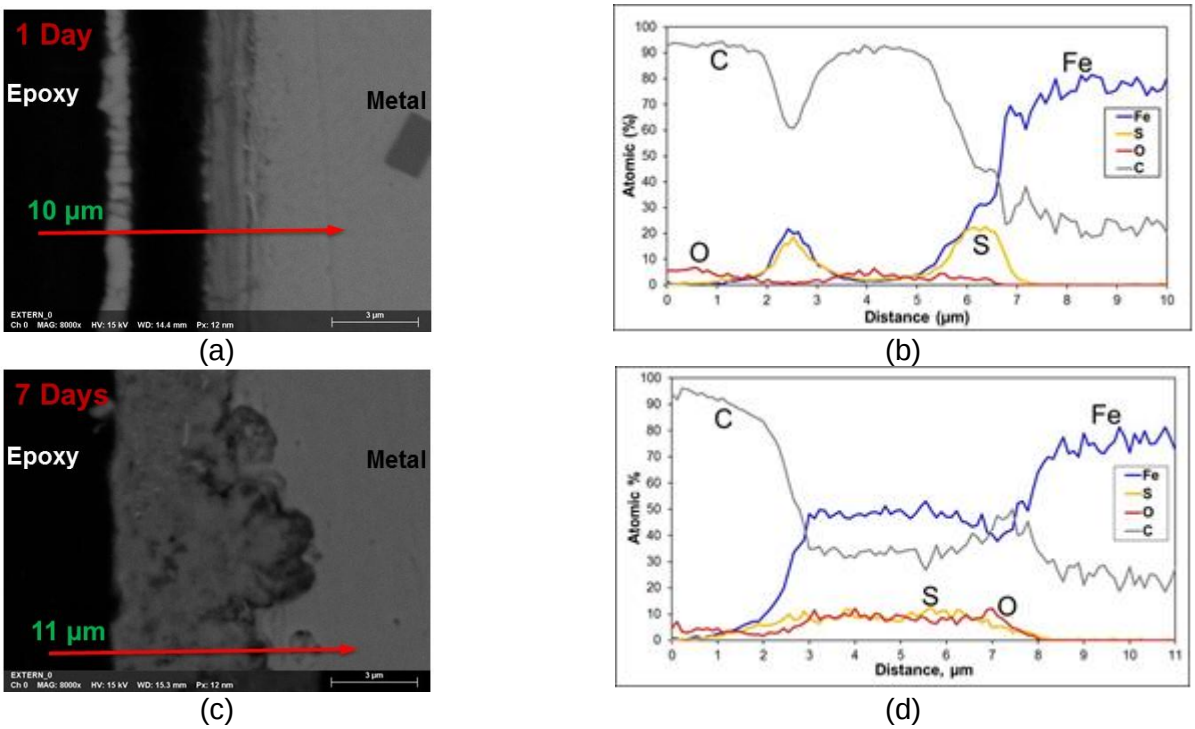

Figure 12: SEM/EDS analysis of scales formed in two different FTMA experiments with Fraction A1 (TAN = 8.30, S = 0.75 wt.%) at 343°C, 24 h experiment (a)&(b) and 168h experiment (c)&(d)

Comparison of the SEM/EDS analyses for the 24h and 168h tests using fraction B1 is presented in Figure 13. The scale formed during the 24h was thick and consisted of two distinct layers as shown in the SEM image Figure 13(a). The inner layer is much thicker than the outer one, and is mainly formed of iron oxide as the EDS scanning detected O and Fe in this region, Figure 13(b). S and Fe were detected in the region that corresponds to the outer layer; therefore, it can be considered that the scale formed with B1 had an inner oxide layer with an FeS layer on top of it. The EDS scanning analysis of the 168h scale - Figure 13(d) - found that it also consisted of a mixture of iron oxide and FeS. The SEM image of the 168h scale revealed that it was thinner than in the 24h test, while the multilayered structure was not as evident as in the former case. However, the thin scale formed in the longer test

with B1 was very protective and the corrosion rate was much lower than in the 24h test of the same fraction.

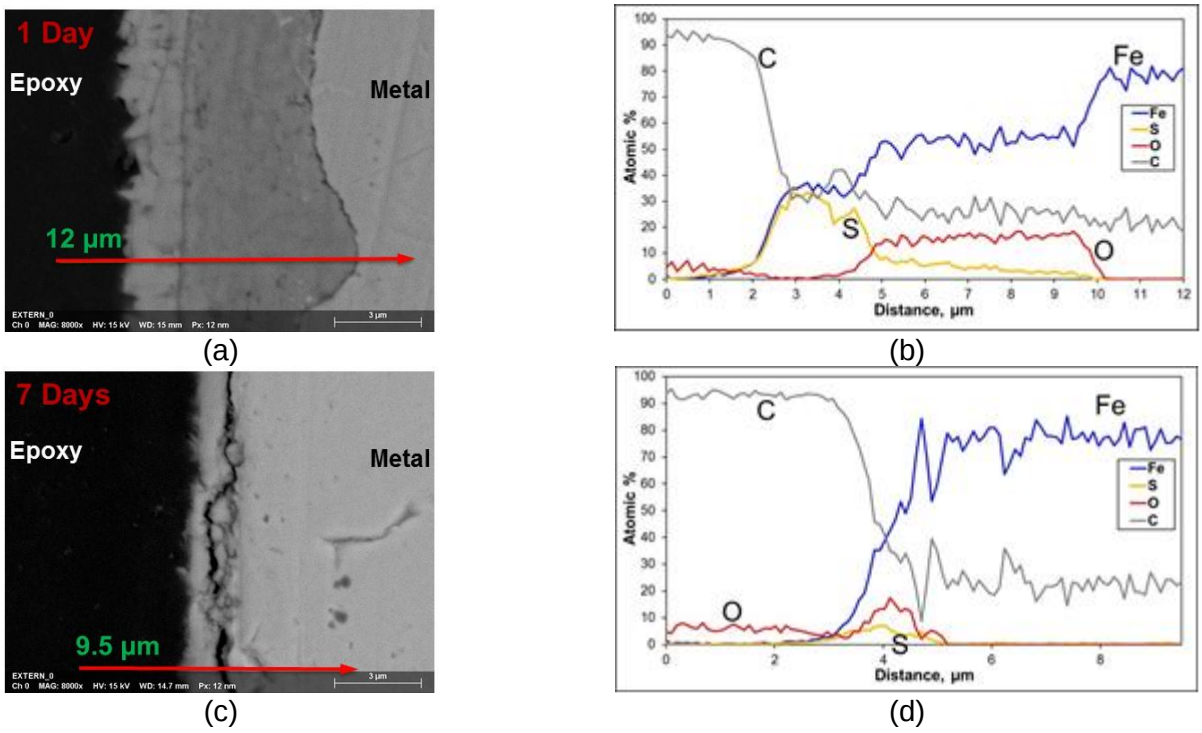

Figure 13: SEM/EDS analysis of scales formed in two different FTMA experiments with Fraction B1 (TAN = 2.77, S = 1.35 wt.%) at 343°C, 24h experiment (a)&(b) and 168h experiment (c)&(d).

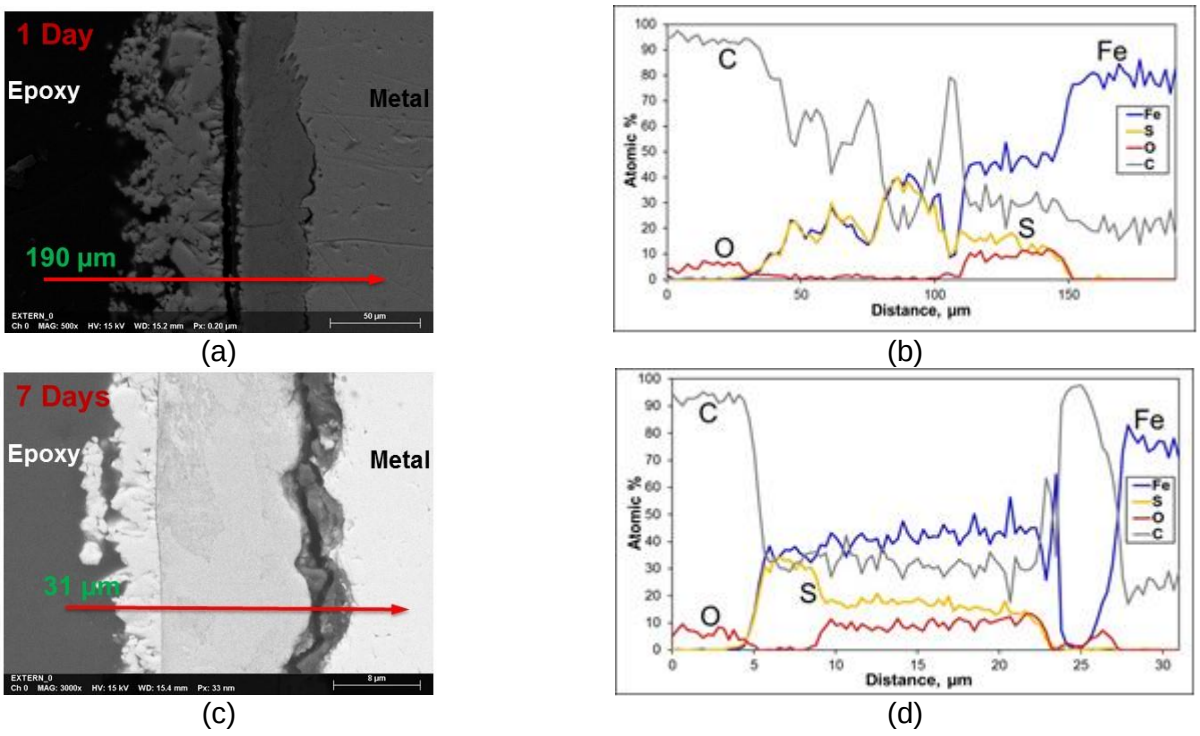

Figure 14: SEM/EDS analysis of scales formed in two different FTMA experiments with Fraction C1 (TAN = 1.51, S = 1.92 wt.%) at 343°C, 24 h experiment (a)&(b) and 168h experiment (c)&(d).

The SEM/EDS analysis was applied also to the scales formed with fraction C1 in the 24h and 168h experiments. Comparison of these two scales analysis is presented in Figure 14. The EDS scanning analysis, Figure 14(b), of the 24h scale indicates that the two layers shown in the SEM image of this scale (a) have different chemical compositions. Thus, O, S, and Fe were found in the inner layer, which suggests it consists of a mixture of iron oxide and FeS. For the outer layer, the EDS analysis found only S and Fe, which indicates it was made of FeS. For the scale formed in the 168h test, the EDS analysis (Figure 14(d)) found a similar chemical composition and distribution of the elements in the successive scale layers. The inner layer was a complex mixture of iron oxide and FeS and the outer layer consisted only of FeS.

The EDS analysis indicates that the oxide layer that was formed in scales generated both in short tests (24h) and in long tests (168h). However, the corrosion rates comparisons of these tests indicate that the oxide layer formation cannot be correlated with scales protectiveness or with the lack of it.

CONCLUSIONS

The influence of time duration on crude fractions corrosivity was evaluated in experiments using three different VGO fractions and performed in a special “flow through” apparatus, the FTMA (Flow Through Mini Autoclave). All experiments were carried out at the same temperature of 343°C, under continuous flow conditions, and had specific time durations *i.e.* 24, 48, 72, and 168h. For all three selected VGO fractions labeled as A1 (TAN – 8.30, S – 0.75 wt.%), B1 (TAN – 2.77, S – 1.35 wt.%), and C1 (TAN – 1.51, S – 1.92 wt.%), corrosion rates decrease as the experimental time increases. For the same time duration experiments, the VGO corrosivity increased with their S-content, suggesting that the corrosive effect of S was dominant over the NAP acids.

Aside from measuring the corrosion rates in experiments with different time durations, the current study also generated some analytical data. XRF analyses (S and Fe concentrations) obtained for one fraction (A1) suggested that initial reactions of S and NAP acids with the metal were very intense but then decreased slowly in the next 6 hours and reached values closer to the initial ones for the rest of the test duration. A similar evolution of acid and sulfur was observed in TAN and XRF analyses for samples collected periodically of all three fractions.

SEM images of cross sections for all exposed CS specimens indicate that the scales had a multilayered structure. The scale thickness increases with time for fraction A1 and decreases for fraction B1. For fraction C1, the SEM analysis suggests that this VGO forms the thickest scale in 24h and in 168h experiments. For all VGO cases, the EDS specimen analysis indicates that the scales are mainly composed of iron sulfide (FeS), though an iron oxide layer was also detected especially in long-term experiments. The presence of an iron oxide layer detected in most of the scales formed in these experiments could not be correlated with the scales protective properties and with the corrosivity of the three selected crude fractions. Further works (experimental and analytical) are being carried out in laboratory to clearly elucidate the scale properties and changes in corrosivity for the considered VGO fractions.

ACKNOWLEDGEMENTS

Authors are thankful to sponsors of Naphthenic Acid Corrosion Joint Industry Project (NAP JIP) for financially supporting this research project at the Institute for Corrosion and Multiphase Technology, Ohio University, USA and allowing us to publish the results obtained from the on-going experimental work.

REFERENCES

1. H.A. Cataldi, R.J. Askevold, A.E. Harnsberger, “Estimating the corrosivity of crude oils,” *Petroleum Refiner*, 32, 7 (1953), p. 146.

2. W.A. Derungs, “Naphthenic acid corrosion - an old enemy of the petroleum industry,” *Corrosion*, 12, (1956), p. 617.

3. E. Slavcheva, B. Shone, A. Turnbull, “Review of naphthenic acid corrosion in oil refining,” *Br Corrosion J*, 34, (1999), p. 125.

4. H.L. Craig Jr., “Temperature and velocity effects in naphthenic acid corrosion,” CORROSION/1996, paper No. 603, (Houston, TX: NACE, 1996).

5. D.R. Qu, Y.G. Zheng, H.M. Jing, Z.M. Yao, W. Ke, “High temperature naphthenic acid corrosion and sulphidic corrosion of Q235 and 5Cr1/2Mo steels in synthetic refining media,” *Corros Sci*, 48, (2006), p. 1960.

6. G. Bota, Y. Kurapati, P.Jin, W. Robbins, “Sulfur/TAN ratio effect on iron sulfide (FeS) scale properties challenged in continuous oil flow,” CORROSION/2019, paper No. 13490, (Nashville, TN: NACE, 2019).

7. S.D. Kapusta, A. Ooms, A. Smith, F. Van den Berg, W. Fort, “Safe processing of acid crudes,” CORROSION/2004, paper no. 04637 (Houston, TX: NACE, 2004).

8. E. Babaian-Kibala, H.L. Craig Jr., G.L. Rusk, K.V. Blanchard, T.J. Rose, B.L.Uehlein, R.C. Quinter, M.A. Summers, “Naphthenic acid corrosion in refinery settings,” *Mater Perform*, 32, (1993), p. 50.

9. P. Jin, W. Robbins, G. Bota, “Effect of temperature on scale formation in high temperature corrosion by model naphthenic acids and sulfur compounds under replenishing conditions.” *Energy Fuels*, 31, (2017), p. 10222.

10. P. Jin, W. Robbins, G. Bota, “High temperature corrosion by carboxylic acids and sulfidation under refinery condition - Mechanism, model, and simulation,” *Ind Eng Chem Res*, 57, (2018), p. 4329.

11. P. Jin, G. Bota, W. Robbins, S. Nesic, “Analysis of oxide scales formed in the naphthenic acid corrosion of carbon steel,” *Energy Fuels*, 30, 8 (2016), pp. 6853.

12. H.D. Dettman, N. Li, D. Wickramasinghe, J. Luo, “The influence of naphthenic acid and sulphur compound structure on global crude corrosivity under vacuum distillation conditions,” CORROSION/2012, paper no. 0001326, (Salt Lake City, UT: NACE, 2012).

13. A. Turnbull, E. Slavcheva, B. Shone, “Factors controlling naphthenic acid corrosion,” Corrosion, 54, (1998), p. 922.

14. P. Jin, S. Nesic, “Mechanism of magnetite formation in high temperature naphthenic acid corrosion by crude oil fractions,” *Corros Sci*, 115, (2017), p. 93.

15. ASTM D 4294, "Standard test method for sulfur in petroleum and petroleum products by energy-dispersive X-ray fluorescence spectroscopy," ASTM International, West Conshohocken, PA, (2003).

16. ASTM D664, “Standard test method for acid number of petroleum products by potentiometric titration,” ASTM International, West Conshohocken, PA, (2018).

17. ASTM G 1-90, “Standard Practice for Preparing, Cleaning, and Evaluating Corrosion Test Specimens,” West Conshohocken, PA, Annual Book of ASTM Standards, ASTM, (2011).